Scaling behaviour of cohesive granular flows

Nicolas Berger, Émilien Azéma, Jean-François Douce, Farhang Radjai

A Letters Journal Exploring the Frontiers of Physics

December 2015

EPL, **112** (2015) 64004 www.epljournal.org
doi: 10.1209/0295-5075/112/64004

Scaling behaviour of cohesive granular flows

Nicolas Berger[1,4], Emilien Azéma[1,3], Jean-François Douce[4] and Farhang Radjai[1,2]

[1] *Laboratoire de Mécanique et Génie Civil (LMGC), Université de Montpellier, CNRS - Montpellier, France*
[2] *⟨MSE⟩², UMI 3466 CNRS-MIT, MIT, Massachusetts Institute of Technology - 77 Massachusetts Avenue, Cambridge, MA 02139, USA*
[3] *Chiang Mai University, Faculty of Engineering, Department of Mechanical Engineering - 239 Huay Kaew Rd., Chiang Mai 50200, Thailand*
[4] *ArcelorMittal Research SA - Voie Romaine - 57280 Maizières-lès-Metz, France*

received 12 November 2015; accepted in final form 22 December 2015
published online 12 January 2016

PACS 45.70.-n – Granular systems
PACS 81.05.Rm – Porous materials; granular materials
PACS 61.43.Hv – Fractals; macroscopic aggregates (including diffusion-limited aggregates)

Abstract – The shear strength of dense granular flows is generally described by an effective friction coefficient, ratio of shear to normal stress, as a function of the inertial number I. However, this ratio depends on the normal stress when the particles interact via both friction and adhesion forces, and in this sense it does not properly represent a Coulomb-like friction. For the same reason, it is not a unique function of I. We used extensive contact dynamics simulations to isolate the cohesive strength from the purely frictional strength in dense inertial flows for a broad range of shear rates and adhesion forces between particles. Remarkably, while the frictional part of the strength increases with I, the cohesive strength is found to be a decreasing function of I. We show that a single dimensionless parameter, combining interparticle adhesion with I, controls not only the cohesive strength but also the packing fraction and granular texture in inertial flows.

Cohesive granular flows are essential in all industrial processes dealing with fine powders [1–5] and in natural flows such as landslides and snow avalanches [6–11]. The action of adhesion forces, irrespectively of their origin (capillary, van der Waals, ...), endows granular flows with a cohesive strength in addition to the generic frictional strength that stems from friction forces and inelastic collisions between particles [4,5,12–28].

In the quasi-static regime, the shear strength of cohesive granular materials is classically expressed by the relation

$$\tau = \tan\varphi\,\sigma_n + c, \tag{1}$$

where φ is the effective friction angle, σ_n is the normal stress and c is the cohesion of the material, which simply represents the shear stress at zero normal stress [24,29,30]. In noncohesive granular materials, the friction coefficient $\mu = \tan\varphi$ is an increasing function of the inertial number defined by [31–36]

$$I = \dot{\gamma}\langle d\rangle \left(\frac{\rho}{\sigma_n}\right)^{1/2}, \tag{2}$$

which represents the ratio of shear rate $\dot{\gamma}$ to the characteristic relaxation rate $(\sigma_n/\rho)^{1/2}/\langle d\rangle$, where $\langle d\rangle$ is the mean particle diameter and ρ is the density of particles. Rognon *et al.* used numerical simulations with a simple adhesion law to investigate the effect of cohesion on this $\mu(I)$ rheology [11,37]. They defined an "apparent friction" coefficient μ_a as in noncohesive granular materials by the ratio $\mu_a = \tau/\sigma_n$, and numerically determined its dependence on both I and a dimensionless adhesion index η, thereby extending the rheology of inertial flows to cohesive granular materials.

The conceptual drawback of the above analysis is that μ_a is dependent on the load level σ_n due to the presence of adhesion forces, and in this sense it does not represent a Coulomb-like friction coefficient. For the same reason, μ_a is not a unique function of I. In fact, eq. (1) simply states that the real friction coefficient μ (independent of the load level) is given by subtracting the macroscopic cohesion c from the shear stress τ before normalizing by the normal stress σ_n. This means that the cohesive granular flows in the inertial regime should be characterized by both a friction coefficient μ and a macroscopic cohesion c, as two independent strength parameters of the flow, and the rheology must be described by two distinct functions $\mu(I)$ and $c(I,\eta)$.

The idea of this paper is to determine the function $c(I,\eta)$, as well as the packing fraction $\nu(I,\eta)$, from discrete-element simulations. Our simulation data indicate that c scales with η and it declines nearly logarithmically with I. Furthermore, considering the packing fraction and several descriptors of the contact network such as coordination number and contact anisotropy, we obtain an excellent data collapse by changing the control parameter from I to a dimensionless number I_c that combines inertial and adhesion forces. This new scaling implies that different combinations of adhesion and shear rate for the same value of I_c yield similar contact networks and thus the same cohesive strength.

The simulations were performed by means of the contact dynamics method [38–40] with $N_p = 8000$ disks (in 2D) of density ρ with diameters d distributed within a range $[d_{min}, d_{max}]$ with $d_{max} = 10d_{min}$ and a uniform distribution of particle volumes. This size distribution is broad enough to prevent from pathological geometrical ordering in 2D [41]. In modeling noncohesive materials this is achieved by a lower-size polydispersity, but cohesion between particles tends to enhance the correlations. A uniform distribution of particle volumes with a high-size ratio, which is often also the case of most naturally occurring granular matter such as soils, has the advantage to allow for efficient pore-filling and thus a locally amorphous structure. The friction coefficient μ_s between particles was set to 0.4. Both normal and tangential restitution coefficients were set to zero. In fact, the restitution coefficients have little influence on dense granular flows as long as they are below 0.8 since inelastic collisions occur at high frequency and dissipate the kinetic energy at time scales much shorter than those of the imposed shear rate and particle relaxation under the imposed confining pressure [42]. Moreover, the adhesion forces between particles also cancel the restitution of kinetic energy upon collisions. The adhesion force f_c between two particles i and j was modelled by a generic expression $f_c = 2\pi\chi\sqrt{R_iR_j}$, where χ is homogeneous to a surface energy ("line energy" in 2D) and $\sqrt{R_iR_j}$ is the reduced radius of the two particles [19,24,43,44]. This expression represents either a surface force resulting from van der Waals forces between two smooth particles or a capillary force. In both cases, it is assumed that the force is short-ranged and acts only at contact points.

A geometrical procedure was used to confine the particles in the simulation box with periodic boundaries in the horizontal direction and a normal stress σ_n applied on the top wall; see fig. 1. The gravity was set to zero to avoid stress gradients. The bottom wall was fixed and the packing was sheared by imposing a constant horizontal velocity v_x on the top wall. After a transient, a steady flow state is reached with a nearly constant packing fraction ν depending on the shear rate $\dot\gamma$, confining stress σ_n and adhesion f_c between particles. Hence, two dimensionless parameters govern the flow. In analogy with noncohesive granular flows, the first parameter is the inertial number I. The second parameter is the "adhesion index" defined by [20,22–24]

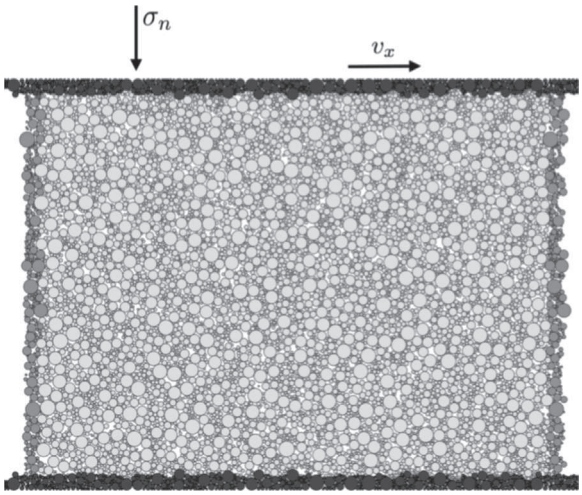

Fig. 1: Plane shear simulation. Black particles compose the rough walls. The periodic left-right boundaries are marked by gray particles.

$$\eta = \frac{f_c}{\sigma_n\langle d\rangle}, \tag{3}$$

which represents the degree of adhesion as compared to the typical repulsive force $\sigma_n\langle d\rangle$ between particles induced by the confining stress. The effects of system parameters χ, $\langle d\rangle$, σ_n and $\dot\gamma$ on the flow are expected to be expressed only through the dimensionless parameters I and η. An interesting issue is whether flow properties, such as cohesion and packing fraction, scale with a single parameter combining I and η.

We performed several series of simulations by varying I from 10^{-3} to 0.35 for $\eta = 0$ (noncohesive) $\eta = 5$, 10, 15 and 20. For this range of values of η, the whole packing is sheared and $\dot\gamma$ represents the mean shear rate. We simulated also larger values of η (> 20) but the flow developed systematically shear bands often in the vicinity of the driving wall. Indeed, at such high levels of cohesion, the particles are strongly correlated and the wall effects are expected to prevail. Video samples of the simulations analysed in this paper can be found following this link: `www.cgp-gateway.org/ref031`.

We measured the stresses from the principal values σ_1 and σ_2 of the stress tensor $\sigma_{\alpha\beta} = n_c\langle\ell_\alpha f_\beta\rangle$, where n_c is the number density of force-bearing contacts, ℓ_α is the α-component of the branch vector joining the centers of two particles sharing a contact and f_β is the β-component of the corresponding contact force [45–48]. The average $\langle\ldots\rangle$ runs over all contacts inside the control volume, which is the simulation cell in exception to the a few particle layers next to the top and bottom walls.

Moreover, since we work with stress invariants σ_1 and σ_2, we define the friction coefficient μ' and friction angle φ' from the stress deviator $q = (\sigma_1 - \sigma_2)/2$ and average stress

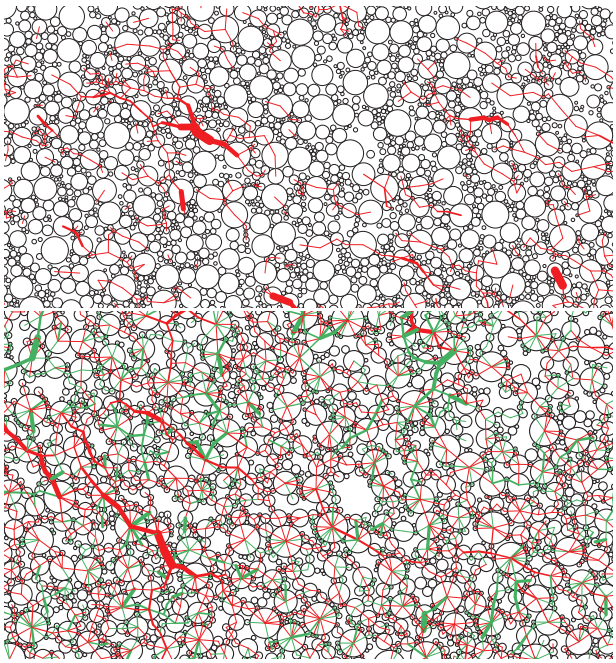

Fig. 2: (Color online) Two snapshots of sheared granular packings in the steady state for $I = 0.23$, $\eta = 0$ (top) and $I = 0.03$, $\eta = 15$ (bottom). The line thickness is proportional to the normal force.

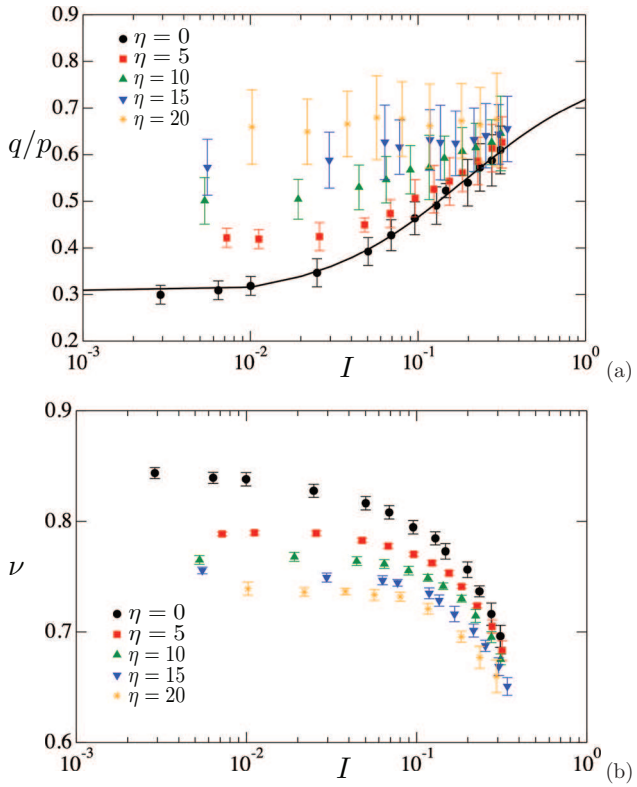

Fig. 3: (Color online) Normalized stress deviator (a) and packing fraction (b) as a function of inertial number for different values of the adhesion index. The error bars represent the standard deviation over 200 records of the flow in the steady state. The solid line is experimentally suggested fit to the data; see text.

$p = (\sigma_1 + \sigma_2)/2$. We have $\mu' = \sin\varphi' = q/p$ according to the Mohr-Coulomb construction. It is worth noting that in steady shear flow the normal stress difference vanishes and we have $\mu' \simeq \mu$ but $\varphi' \neq \varphi$ by construction. Hence, from the canonic definition of cohesion c, we have [24]

$$q(\eta, I) = p \sin\varphi'(I) + c(\eta, I)\cos\varphi'(I). \tag{4}$$

In this writing, it is assumed that the effective friction angle has a Coulombic nature and is therefore independent of the confining stress and adhesion force. This allows us to obtain the normalized cohesion c/p for given values of η and I:

$$\frac{c}{p}(\eta, I) = \frac{1}{\cos\varphi'(I)}\frac{q}{p}(\eta, I) - \mu(I), \tag{5}$$

The friction angle $\varphi'(I) = \sin^{-1}[q/p(0, I)]$ is simply the stress ratio $q/p(0, I)$ of a noncohesive packing ($\eta = 0$).

Figure 2 displays two snapshots of the sheared packing: a noncohesive flow with high inertia ($I = 0.23$ and $\eta = 0$) and a highly cohesive flow with low inertia ($I = 0.03$ and $\eta = 15$). Both flows are considerably looser than a quasi-static noncohesive flow due to inertia in the first case and as a result of the action of adhesion forces in the second case. This is suggestive of the scaling that will be discussed in detail below. Note that, in contrast to the noncohesive flow, nearly all particles stick to one another and only a few particles are floating in the cohesive case.

Figure 3 shows q/p and packing fraction ν as a function of I for different values of η. The data are averaged in the steady state for a total cumulative shear strain ranging from $\gamma = 10$ for $I = 10^{-3}$ to $\gamma = 10^3$ for $I = 0.35$. q/p is an increasing function of η for all values of I. It increases with I for all values of η except for $\eta = 20$ where it keeps a nearly constant level. All data points are above the internal friction coefficient $\mu(I)$, which is well fitted by the experimentally suggested functional form [49,50]

$$\mu(I) = \mu_1 + \frac{\mu_2 - \mu_1}{1 + I_0/I} \tag{6}$$

with $\mu_1 \simeq 0.29$, $\mu_2 \simeq 0.80$ and $I_0 \simeq 0.19$. At high inertia, the values of q/p in cohesive flows converge towards $\mu(I)$. The packing fraction ν shows opposite trends as a function of I and η.

Figure 4 shows the normalized cohesion $c/(p\eta)$, extracted from the data displayed in fig. 3 by means of eq. (5), as a function of I. We see that, within statistical fluctuations, the macroscopic cohesion, normalized by average stress p, scales with adhesion index η and declines as I increases. In particular, we have $c/(p\eta) \equiv k_0 \simeq 0.02$ in the quasi-static limit ($I \to 0$) and it vanishes in highly inertial flows. Note that, since $p \simeq \sigma_n$, we have $k_0 \simeq c(I = 0)\langle d\rangle/f_c$ and its constant value mainly reflects the number density of contacts n_c in the force network [19]. n_c is

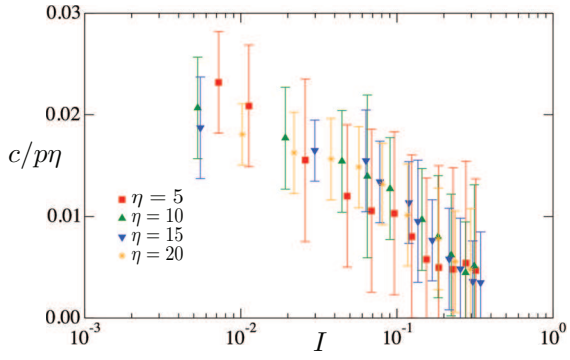

Fig. 4: (Color online) The cohesive strength normalized by average stress p and adhesion index η, as a function of the inertial number for different values of η. The error bars reflect those of q/p in fig. 3.

proportional to both the coordination number Z and ν. In the same way, the decrease of cohesion with the inertial number may be attributed to the fast decrease of the coordination number Z as shown in fig. 5. The values of Z are approximately the same in cohesive flows but differ from those in noncohesive flows where floating particles are always present and increase in number (from 0.35 to 0.75) as I increases from 10^{-3} to 0.35 [35]. In cohesive flows the proportion of floating particles increases from nearly zero to 0.2. The contact anisotropy a_c, defined by a truncated Fourier expansion $P(\theta) = [1 + a_c \cos 2(\theta - \theta_c)]/\pi$ of the proportion $P(\theta)$ of contacts oriented along θ, increases with I. The increase of a_c with I is at the origin of the increase of μ with I [35].

The simulation results presented above reveal the scaling of c/p with η and its slow falloff as I increases. But ν, Z and a_c do not collapse on a single curve as a function of I for different values of η. These quantities are related to the force-bearing contact network and hence expected to be controlled by a combination of I and η. In fact, the definition of the inertial number by eq. (2) assumes that the relaxation rate depends only on the confining stress σ_n. In cohesive flows, however, the effect of adhesion is to increase the relaxation rate by enhancing local stresses acting on the particles. The stresses being additive, we thus have to add the cohesive stress $f_c/\langle d\rangle$ to σ_n. However, since $f_c/\langle d\rangle$ represents only an order of magnitude of the cohesive stress, it should be weighted by a coefficient α accounting for the structure of the packing or the details of dissipation mechanisms during flow. A similar approach was used for the scaling of shear stresses in dense suspensions where the fluid and grain stresses are both responsible for the effective friction angle and effective viscosity of the mixture [51]. Accordingly, we obtain a modified inertial number

$$I_c = \dot{\gamma}\langle d\rangle \left(\frac{\rho}{\sigma_n + \alpha f_c/\langle d\rangle}\right)^{1/2} = \frac{I}{(1+\alpha\eta)^{1/2}}. \quad (7)$$

Figure 6 displays our data points plotted as a function of I_c with $\alpha = 0.08$. We observe a nice collapse of the data

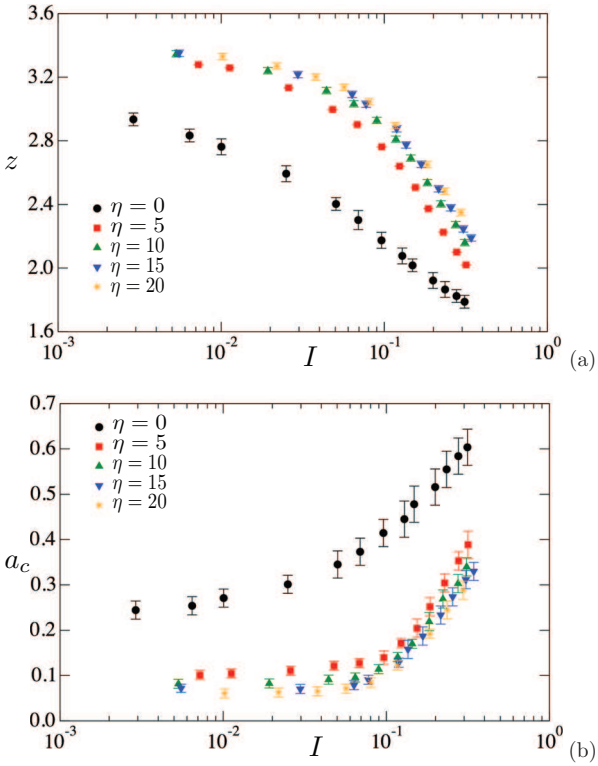

Fig. 5: (Color online) Evolution of the coordination number (a) and contact anisotropy a_c (b) as a function of the inertial number for different values of the adhesion index.

points in cohesive flows for Z and a_c. The finite difference with the data corresponding to the noncohesive flow reflects the increasing number of floating particles. We also observe an improved data collapse for c/p, specially at high values of I_c. These data are well fit to a logarithmic function

$$\frac{c}{p} = \frac{k_0\eta}{1 - \beta\ln(1 - I_c)} \quad (8)$$

with $\beta \simeq 6.4$. Regarding the packing fraction, the data points collapse when they are normalized by the packing fraction $\nu_{max}(\eta) = \nu(\eta, I = 0) \simeq \nu_{max}(0)/(1 + \eta/\eta_0)$ with $\eta_0 \simeq 150$. This means that the adhesion index affects the rheological behavior of inertial flows described in terms of c/p and ν through both its effect in the quasi-static limit and its value in the expression of the cohesive inertial number I_c.

Finally, we get an analytical estimate of q/p as a function of I_c for different values of η by introducing the expressions (8) and (6) in eq. (4) with the definition of I_c given by eq. (7). The q/p data are plotted in fig. 7 as a function of I_c for all values of η, together with their analytical estimates. We see that the predicted trends are in excellent quantitative agreement with the data.

The above findings, obtained by means of extensive simulations for a broad range of inertia and adhesion forces, provide a consistent framework for the description of macroscopic cohesion in inertial granular flows.

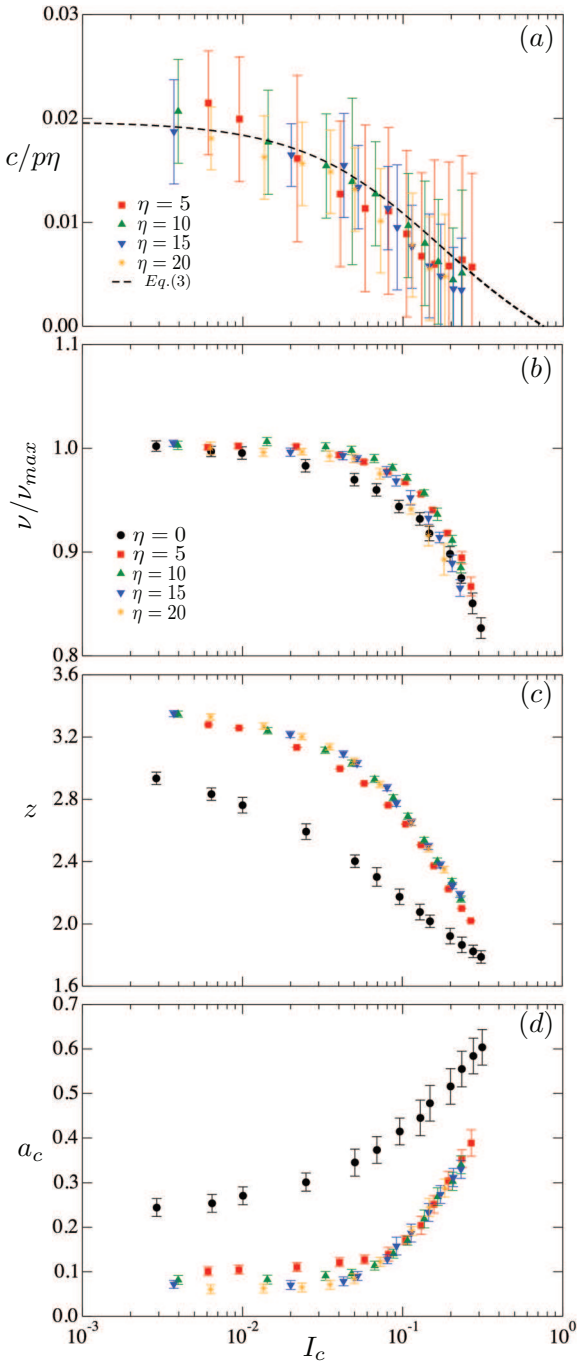

Fig. 6: (Color online) Evolution of normalized cohesion (a), normalized solid fraction (b), coordination number (c) and contact network anisotropy (d) with cohesive inertial number. The dashed line in (a) is the logarithmic fitting form of eq. (8).

The cohesive strength, as a strength parameter of granular materials independent of frictional strength, scales with the adhesion index and declines logarithmically as a function of the cohesive inertial number I_c that incorporates the effect of adhesion on the internal relaxation rate. In a similar vein, the granular texture, characterized by coordination number and contact network anisotropy, is a function only of the cohesive inertial number. Since the latter combines the inertial number and adhesion index, the above scaling suggests that the effect of adhesion forces is quite similar to that of particle inertia. Both parameters lead to reduced packing fraction and enhanced shear strength. The evolution of the total shear strength with I_c reflects therefore the competing contributions of friction coefficient, as an increasing function of I_c, and cohesive strength, as a decreasing function of I_c. The force distributions, contact network connectivity and force anisotropy of cohesive flows are consistent with this picture and will be published elsewhere.

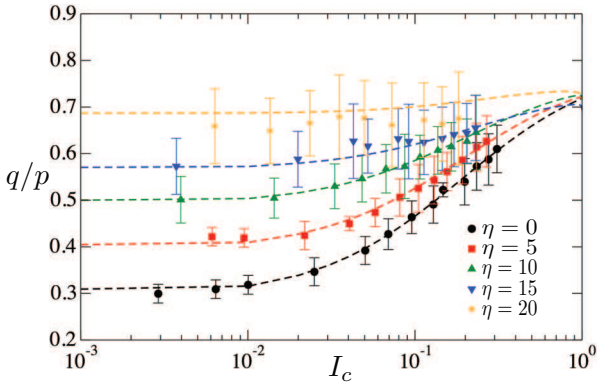

Fig. 7: (Color online) Normalized shear stress as a function of the cohesive inertial number. The lines represent analytical estimates for each value of the adhesion index; see text.

* * *

The authors acknowledge financial support by ArcelorMittal. FR would also like to acknowledge the support of the ICoME2 Labex (ANR-11-LABX-0053) and the A*MIDEX projects (ANR-11-IDEX-0001-02) cofunded by the French program Investissements d' Avenir.

REFERENCES

[1] Mikami T., Kamiya H. and Horio M., *Chem. Eng. Sci.*, **53** (1998) 1927.
[2] Bika D., Gentzler M. and Michaels J., *Powder Technol.*, **117** (2001) 98.
[3] Forrest S., Bridgwater J., Mort P. R., Litster J. and Parker D. J., *Powder Technol.*, **30** (2002) 91.
[4] Bocquet L., Charlaix E. and Restagno F., *C. R. Phys.*, **3** (2002) 207.
[5] Miclea C., Tanasoiu C., Miclea C. F., Sima F. N. and Cioangher M., *Influence of forming pressure of compacted powders on densification of sintered body*, in *Proceedings of Powders and Grains 2005*, edited by Garcia-Rojo R., Herrmann H. J. and McNamara S. (A. A. Balkema, Leiden, The Netherlands) 2005, pp. 655–658.
[6] Iveson S., Beathe J. and Page N., *Powder Technol.*, **127** (2002) 149.
[7] Liu S. H., Sun D. A. and Wang Y., *Comput. Geotech.*, **30** (2003) 399.

[8] Kim T. and Hwang C., *Eng. Geol.*, **69** (2003) 233.
[9] Jiang M. J., Leroueil S. and Konrad J. M., *Comput. Geotech.*, **31** (2004) 473.
[10] Naaim M., Naaim-Bouvet F., Faug T. and Bouchet A., *Cold Regions Sci. Technol.*, **39** (2004) 193.
[11] Rognon P., Roux J.-N., Naaim M. and Chevoir F., *J. Fluids Mech.*, **596** (2008) 21.
[12] Mason T. G., Levine A., Ertas D. and Halsey T. C., *Phys. Rev. E*, **60** (1999) R5044(R).
[13] Lu N. and Likos W., in *Proceedings of Poromechanics V* (ASCE) 2013, pp. 1669–1675, doi: 10.1061/9780784412992.197.
[14] Bocquet L., Charlaix E., Ciliberto S. and Crassous J., *Nature*, **396** (1998) 735.
[15] Fraysse N., Thomé H. and Petit L., *Eur. Phys. J. B*, **11** (1999) 615.
[16] Voivret C., Radjai F., Delenne J.-Y. and El Youssoufi M. S., *Phys. Rev. Lett.*, **102** (2009) 178001.
[17] Delenne J.-Y., Richefeu V. and et Radjai F., *J. Fluid. Mech. Rapids*, **762** (2015) R5.
[18] Saint-Cyr B., Radjai F., Delenne J.-Y. and Sornay P., *Phys. Rev. E*, **87** (2013) 052207.
[19] Richefeu V., El Youssoufi M. and Radjai F., *Phys. Rev. E*, **73** (2006) 051304.
[20] Khamesh S., Roux J.-N. and Chevoir F., *Phys. Rev. E*, **92** (2015) 022201.
[21] Valverde J. M. and Castellanos A., *Europhys. Lett.*, **75** (2006) 985.
[22] Gilabert F., Roux J.-N. and Castellanos A., *Phys. Rev. E*, **78** (2008) 031305.
[23] Richefeu V., El Youssoufi S., Azéma E. and Radjai F., *Powder Technol.*, **190** (2009) 258.
[24] Radjaï F. and Richefeu V., *Philos. Trans. R. Soc. A*, **367** (2009) 5123.
[25] Estrada N., Lizcano A. and Taboada A., *Phys. Rev. E*, **82** (2010) 011303.
[26] Luding S. and Alonso-Marroquin F., *Granular Matter*, **13** (2011) 109.
[27] Fiscina J. E., Pakpour M., Fall A., Vandewalle N., Wagner C. and Bonn D., *Phys. Rev. E*, **86** (2012) 020103.
[28] Pakpour M., Habibi M., Mller P. and Bonn D., *Sci. Rep.*, **2** (2012) 549.
[29] Mitchell J. and Soga K., *Fundamentals of Soil Behavior* (Wiley, New York, NY) 2005.
[30] Fournier Z., Gerimichalos D., Herminghaus S., Kohonen M. M., Mugele F., Scheel M., Schulz M., Schulz B., Schier C., Seemann R. and Shudelny A., *Appl. Phys.: Condens. Matter*, **17** (2005) 477.
[31] GDR-MiDi, *Eur. Phys. J. E*, **14** (2004) 341.
[32] da Cruz F., Emam S., Prochnow M., Roux J.-N. and Chevoir F., *Phys. Rev. E*, **72** (2005) 021309.
[33] Jop P., Forterre Y. and Pouliquen O., *Nature*, **441** (2006) 727.
[34] Börzsönyi T. and Ecke R. E., *Phys. Rev. E*, **76** (2007) 031301.
[35] Azéma E. and Radjaï F., *Phys. Rev. Lett.*, **112** (2014) 078001.
[36] Kamrin K. and Henann D., *Soft Matter*, **11** (2015) 179.
[37] Rognon P. G., Roux J.-N., Wolf D., Naam M. and Chevoir F., *Europhys. Lett.*, **74** (2006) 644.
[38] Moreau J., *Eur. J. Mech. A/Solids*, **13** (1994) 93.
[39] Radjaï F. and Richefeu V., *Mech. Mater.*, **41** (2009) 715.
[40] Azéma E., Estrada N. and Radjaï F., *Phys. Rev. E*, **86** (2012) 041301.
[41] Nguyen D.-H., Azma E., Radjai F. and Sornay P., *Phys. Rev. E*, **86** (2014) 041301.
[42] Staron L. and Hinch E., *Granular Matter*, **9** (2007) 205.
[43] Israelachvili J. N., *Intermolecular and Surface Forces* (Academic Press, London) 1993.
[44] Willett C., Adans M., Johnson S. and Seville J., *Langmuir*, **16** (2000) 9396.
[45] Christoffersen J., Mehrabadi M. M. and Nemat-Nasser S., *J. Appl. Mech.*, **48** (1981) 339.
[46] Moreau J. J., *Numerical investigation of shear zones in granular materials*, in *Proceedings of Friction, Arching, Contact Dynamics*, edited by Wolf D. E. and Grassberger P. (World Scientific, Singapore) 1997, pp. 233–247.
[47] Ouadfel H. and Rothenburg L., *Mech. Mater.*, **33** (2001) 201.
[48] Staron L., Radjai F. and Vilotte J., *Eur. Phys. J. E*, **18** (2005) 311.
[49] Jop P., Forterre Y. and Pouliquen O., *Nature*, **441** (2006) 727.
[50] Forterre Y. and Pouliquen O., *Annu. Rev. Fluid Mech.*, **40** (2008) 1.
[51] Trulsson M., Andreotti B. and Claudin P., *Phys. Rev. Lett.*, **109** (2012) 118305.